Traditional to Modern Antenna Test Environments: The Impact of Robotics And Computational Electromagnetic Simulation on Modern Antenna Measurements

D.M. Lewis[1], J. Bommer[2], G.E. Hindman[3], S.F. Gregson[3]
[1] The Boeing Company, Seattle WA USA, dennis.m.lewis@boeing.com
[2] ANSYS Inc., Southpointe 2600 Ansys Drive, Canonsburg, PA 15317 USA, jason.bommer@ansys.com
[3] Next Phase Measurements LLC., 11521 Monarch St., Garden Grove, CA, USA, greg.hindman@npmeas.com

***Abstract*—Traditional antenna test facilities are designed with a specific measurement application in mind. As a result, these facilities tend to have fixed measurement geometries with much of the range performance analysis being performed only once, during the design phase of the test facilities implementation. Modern antenna measurement ranges employing multi-axis robotic positioners provide a near limitless degree of re-configurability in terms of measurement types and scan geometries. This drives an ongoing need to evaluate each unique setup and application. Model based Systems Engineering and development (MBSE/MBD) approaches can be employed to dramatically reduce the time, effort, and cost associated with the test development and validation phases of a given program. MBSE tools can also be used to optimize test configurations to greatly reduce measurement uncertainties. This paper provides an overview of how these engineering techniques are being harnessed during the implementation of a new dual multi-axis robotic antenna test system.**

***Index Terms*—Antenna measurements, Model Based Systems Engineering, Model Based Development, CEM, Multi-Axis Robot, Near-Field, Extrapolated Gain, Digital Twin.**

I. INTRODUCTION

There are many competing tradeoffs to consider when designing or selecting an antenna test range configuration that will be compatible with current and expected future test and measurement requirements. The challenge of selecting the most appropriate measurement system becomes perhaps even more pronounced when working in research, development, and/or highly advanced manufacturing settings where the system may not be designed for a sole, clearly defined, application. A decision is therefore often made to sacrifice capability or performance to meet budget, space, or time constraints. This paper discuss the design and implementation of a new antenna test system that is predicated on the novel coordinated use of a pair of 6-axis robots which has been greatly aided through the use of Model Based Systems Engineering and Development (MBSE/MBD) [1], and the concept of a Digital Twin (DT) [2]. MBSE/MBD is one of the areas of focus for Boeing's research and in this project, its use was crucial in the successful development of this advanced test system as it enabled various measurement configurations and scenarios to easily be explored and optimized; prior even to the system design being crystalized and the system itself being installed. MBSE/MBD was particularly well suited to this program as the increasing complexity and interdependency of the test systems combined with the demand for a compressed development cycle and lower costs, required a highly robust, efficient, and less error-prone development approach.

Systems incorporating multi-axis robotic positioners, such as that presented herein, are generally capable of acquiring spherical, cylindrical and variable orientation planar near-field data as well as taking far-field and extrapolated gain measurements; with the flexibility of the system meaning the user is not limited to purely these choices [3, 4, 5, 6]. The extreme adaptability of the system affords the test engineer unique opportunities to acquire highly accurate, uniquely tailored measurements, that are not available from other more traditional antenna test systems. However, with this enormous flexibility comes the inherent difficulty of understanding and optimization of the individual modes of operation. This is further compounded by the difficulty of conceiving of all of the intricacies associated with the transition from one measurement mode of operation to another and of conceiving of the practicalities of antenna handling each and every mode, while critically ensuring personnel and equipment safety at all times. This paper will provide an overview of this test system and will highlight the ways in which its evolution was aided and guided by the use of MBSE/MBD.

II. FACILITY OVERVIEW

The new dual 6-axis industrial robotic antenna measurement system is to be situated within a 12.5 x 8 x 5 m [41' x 26' x 17'] (L x W x H) screened anechoic chamber that is heating, ventilation and airconditioned (*i.e.* HVAC controlled) and is lined with 60 cm [24"] pyramidal absorber. Of the two Fanuc multi-axis industrial robots, one is fixed, while the other is installed atop of a 9 m [30'] long linear translation stage. The multi-axis robots are each installed on

pedestals in order to raise the positioners to the centerline of the chamber. This arrangement can be seen illustrated in Fig. 1 below with the stationary robot shown to the left-hand side of the figure, and the moving robot located to the right.

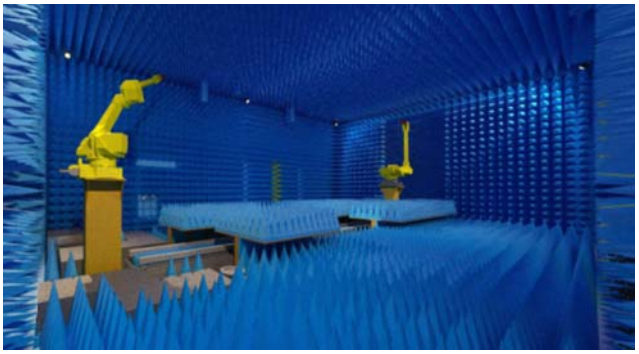

Fig. 1. Illustration of the new dual 6-axis robotic antenna measurement system.

The system, as shown, comprises 14 separate axes that are all under computer control. The two 6-axis robots provide 12 of the motion axes, there is a motorized linear stage under one of the robots and a relatively small floor mounted rotation stage located near the fixed robot which provided the 14th axis. When operated in concert, these axes enable the provision of a range of near-field and far-field test configurations. The primary measurement configurations are summarized in Table 1, with two of the planar near-field (PNF) measurement configurations being illustrated in Fig. 2 below.

TABLE I. DUAL 6-AXIS ROBOTIC ANTENNA MEASUREMENT SYSTEM (DRAMS) PRIMARY CONFIGURATIONS

Configurations	**Axes**		
	Axis 1	***Axis 2***	***Axis 3***
Large Planar – Moving Robot	X: Linear slide	Y: Moving Robot	Pol: Moving Robot
Small Planar – Moving Robot	X: Moving Robot	Y: Moving Robot	Pol: Moving Robot
Small Planar – Stationary Robot	X: Stationary Robot	Y: Stationary Robot	Pol: Stationary Robot
Extrapolation Range	X: Linear slide	N/A	Pol: Moving Robot
Spherical - ϕ/θ	θ: Moving Robot	ϕ: Moving Robot	Pol: Stationary Robot

Fig. 2(a) shows the dual industrial multi axis robots working in concert to take a PNF measurement of a planar array antenna with the acquisition plane inclined by 10° in azimuth and 10° in elevation with respect to the axes of the chamber. This has the advantage that scattering effect within the chamber can be minimized and/or varied so as to optimize and evaluate the facility measurement uncertainty budget. Conversely, Fig. 2(b) presents a more conventional large PNF measurement where the horizontal linear axis is used to increase the size of the acquisition interval which is necessary when testing larger antennas without requiring the use of an excessively large, and expensive, multi-axis robot. Although not shown due to space limitations, each of the primary measurement configurations were simulated, and fully animated, so that the various measurement modes could be understood, verified, and optimized.

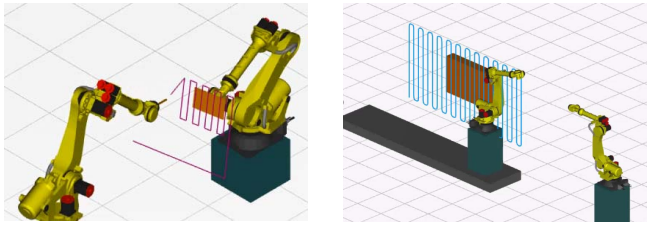

(a) Small inclined PNF Configuration (b) Large PNF Configuration

Fig. 2. Illustration of the new dual 6-axis robotic antenna measurement system.

The relatively complex, 50 GHz, distributed, RF subsystem is based upon a Keysight PNA and remote mixers. This configuration is utilized so as to be able to minimize the loss within the guided wave path so as to maximize the RF power budget in each of the many acquisition modes, *e.g.* PNF, spherical near-field (SNF) and extrapolated gain measurement mode.

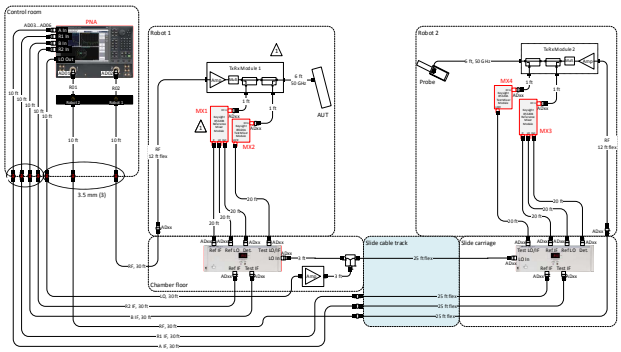

Fig. 3. Illustration of the 50 GHz PNA based distributed RF sub-system for dual robotic antenna measurement system.

Lastly, design for both personnel and equipment safety has been considered. The safety system includes door interlocks, hardware travel limit switches, and laser light fences. Two primary lidar laser light fences are designed into the system. The first and most important system sweeps a horizontal plane and can identify and stop all mechanical axes operations when personnel motion is detected. A second system is primarily designated for hardware safety and is typically oriented in the vertical plane configuration and is intended to prevent the two 6-axis robotic systems from mechanically interfering with one another when operating in the vertical PNF measurement mode.

III. OVERVIEW OF THE APPLICATION OF MBSE/MBD

In this section we illustrate the use of MBSE/MBD with selected examples. As the system is intended to be used as both a conventional antenna test system and an extrapolation gain measurement system, antenna under test (AUT) mounting effects, range reflections, and extrapolation method verification were of significant interest. The first test involved the simulation of a test antenna when installed on one of the multi-axis robots. This arrangement can be seen

presented below in Fig. 4. Here, Fig. 4(a) shows the dipole antenna aligned with the z-axis of the SNF measurement coordinate system. This locates the null of the antenna pattern in the direction of the robotic positioner. Conversely, when mounted as shown in 4(b) this is not the case and consequently, far higher levels of field illuminate the positioner. The equivalent far-field patterns can be seen presented in 4(c) and 4(d). The orientation of the respective patterns is rotated from one another by 90°, which is expected, however the amount of ripple contained within the patterns is also significantly reduced in the *z*-axis orientated case. Although not shown, as a consequence of space restrictions, this simulation was repeated with the AUT being translated in the *z*-axis. Although the mounting of the AUT is unchanged, the positioner itself changes shape and hence the scattering from the changing orientation of the lower positioners does affect the pattern as a consequence of position of the lower stages. Here, the antenna was modelled using the Finite Element Boundary Integral Method (FEBI). The positioner scatters the FEBI source induced currents and this is included within the far-field pattern presented in Fig. 4(c) and 4(d).

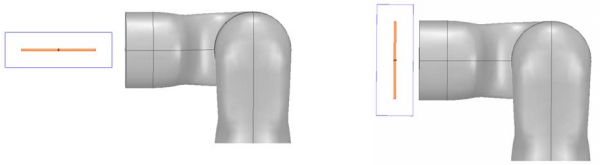

(a) Dipole mounted on positioner aligned with z-axis

(b) Dipole mounted on positioner aligned transverse with the z-axis

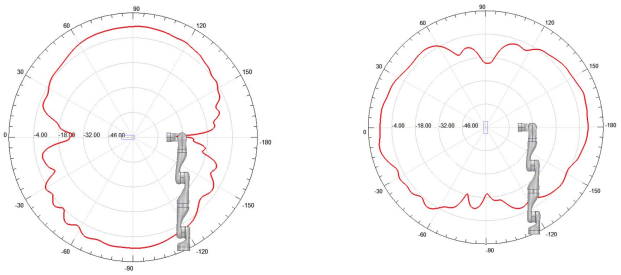

(c) Far-field radiation pattern

(d) Far-field radiation pattern

Fig. 4. Model of low-gain AUT installed on the multi-axis robotic positioner for two different AUT orientations.

The robotic positioning system clearly has an influence on the far-field pattern and consequently the absorber design is of considerable importance. For a positioning system such as this, it is difficult to conceive of a practical absorber layout that will be ideal in all modes of operation. However, the slightly less demanding task of gauging the degree of absorptivity that is needed is an alternative, but still very valuable task. Fig. 5(a) presents a polar plot of the dipole when installed on the robotic positioners in the worst-case orientation. The red trace denotes the ideal free-space far-field pattern whereas the blue trace shows the equivalent pattern with the presence of the perturbing assumed perfect electrical conductor (PEC) positioner. Conversely, Fig 5(b) shows the equivalent result for the case where the exterior surface of the positioner is assumed to be covered with an absorbing material with a reflectivity of -20 dB, which is equivalent to, for example, the performance provided by thin sheet conformal absorber, which is the type of material that may be used with this sort of test system. From inspection of this figure it can be seen that there is a very valuable improvement in the quality of the patterns, *cf.* the region from -90° to +90°, with additional simulations showing that absorber with at least 20 dB of reflectivity should be used. Although not presented herein, further simulations were run in which absorber with 40 dB reflectivity was used together with others that employed more realistic material properties which were modelled using a layered impedance boundary, with the results generally aligning with those summarized here.

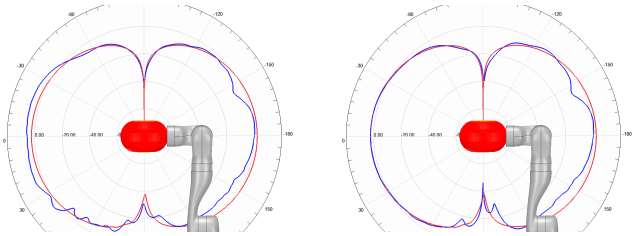

(a) PEC surface

(b) 20 dB surface attenuation

Fig. 5. Dipole AUT mounted on multi-axis robots with a variety of absorber configurations.

The next case that was examined was that of the gain extrapolation method [7, 8]. This was simulated initially using two broadband open-boundary horn antennas and the FEBI method. This can be seen illustrated in Fig. 6 where the S_{21} forward transmission coefficient was plotted as a function of antenna-to-antenna separation that crucially, show the ripple that is an artefact of the mismatch that must be suppressed, *i.e.* filtered out, if reliable extrapolated gain data is to be obtained.

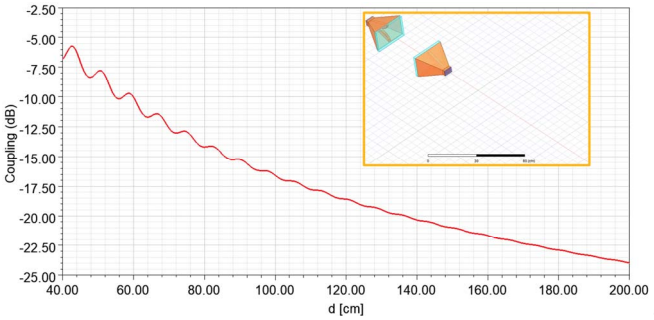

Fig. 6. Gain extrapolation simulation for a single frequency run over a 2 m linear distance using a pair of broadband open-boundary horn antennas.

Next, so that the influence of the anechoic chamber could be examined, and an upper uncertainty bound estimated, the transmission measurement was placed within a 12.5 x 8 x 5 m chamber lined with 60 cm pyramidal absorber. This is an electrically large problem and was therefore tackled using a raytracing-based modelling technique. This simulation was repeated for the case of a perfectly matched layer, and 60 cm tall pyramidal absorber lining. This can be seen presented below in Fig. 7. Here, the magnitude of the ripple that is present on the red trace, which is an artefact of room

reflections, is small compared to the AUT mismatch-ripple that is evident in Fig. 6 above and therefore, for the purposes of validating the extrapolation gain post-processing it may be omitted, at least initially.

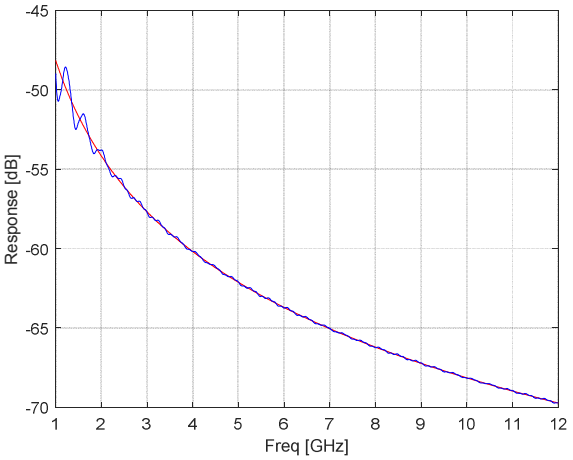

Fig. 7. Plot of the amplitude response in dB from 1 to 12 GHz for a perfect absorber lining and for a chamber lined with 60 cm tall pyramidal absorber.

The first step within the extrapolation gain method is the application of a digital filter which is required to remove the mismatch ripple (and room reflections) that can be seen in Fig. 6 [9, 10] above. Here, the extrapolation measurements were simulated using a computational electromagnetic model (CEM) model of a 0.4 x 0.3 m offset reflector antenna. A spurious mismatch was then incorporated in this model so that the effectiveness of the digital filter, which is needed to suppress antenna-to-antenna standing waves, under a range of different conditions, *e.g.* frequencies, linear acquisition spans, data point spacings, *etc.*, could be explored with the knowledge of a an "absolute truth" model. This can be seen presented in Fig. 8(a) Here, the ideal gain coupling product is denoted by the cyan trace, the antenna-to-antenna standing wave perturbed traces is shown in black, and represents the data that is provided to the digital filter, with lastly the red trace denoting the filtered gain product. It is this digitally filtered data that is used to extrapolate the gain product at ∞. From inspection of Fig. 8(a) it is clear that the agreement between the ideal and filtered data is very encouraging. The reciprocal space plot of the digitally filtered gain product is presented in Fig 8(b) together with the equivalent ideal trace and the quadratic least-squares best fit red curve.

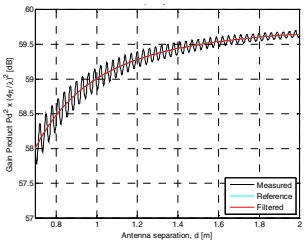

(a) Coupling with and without digital filtering plotted with ideal gain product

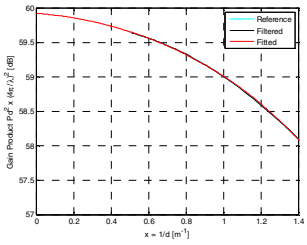

(b) Digital filtered gain product plotted with ideal gain product in reciprocal space

Fig. 8. Plot of the gain product for a pair of antennas, which constitutes a single linear run for the three-antenna gain extrapolation method.

This best fit curve and the extrapolated value represent one of the six data sets that are required by the three-antenna gain method. This process is repeated for the cross-polar case for this pair of antennas. Then, the measurement is repeated with two further combinations of the three antennas whereupon the resulting simultaneous equations are solved so that the gain and polarization properties of the individual antennas can be obtained without a need for further external gain reference data. Based upon the preliminary validation effort that was achieved using simulated "measured" data, the new extrapolated gain post-processing software has recently been verified against an existing reference data set. The presentation of those results will form the subject of a future planned paper.

IV. Example Preliminary PNF Measurements

In this final section, preliminary planar near-field measurements are presented. Fig. 9 below shows a PNF acquisition being taken using the small PNF measurement mode of Table I being performed in an open factory setting, which was part of the preliminary testing.

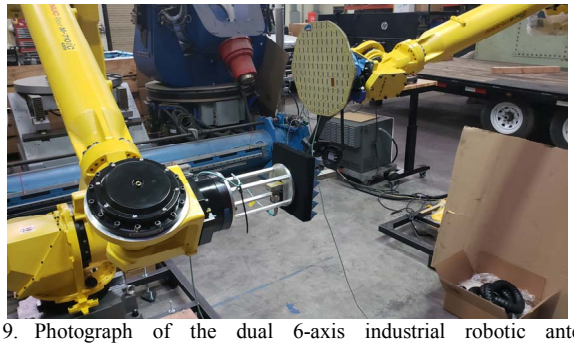

Fig. 9. Photograph of the dual 6-axis industrial robotic antenna measurement system undergoing preliminary factory testing.

Here, the WR 90 open-ended rectangular waveguide probe was installed on one of the Fanuc multi-axis robots with the AUT, which in this case was an *x*-band slotted waveguide circular planar array antenna, being mounted on the second robot. A PNF acquisition was taken and transformed to the far-field using the plane-wave spectrum method [11].

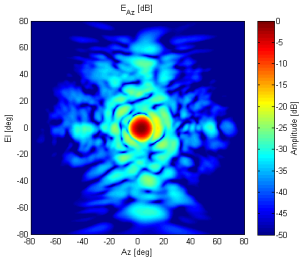

(a) Far-field antenna pattern of x-bend slotted waveguide array antenna

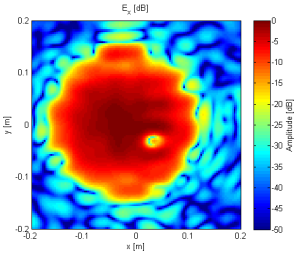

(b) Aperture plane plot of SWGA showing single element covered by conductive tape.

Fig. 10. Antenna pattern measurements of slotted waveguide array antenna acquired using the small PNF measurement configuration.

The equivalent far-field pattern of the array antenna can be seen presented in Figure 10(a) where the field is resolved onto a Ludwig II azimuth over elevation polarization basis and the pattern is tabulated on a corresponding azimuth over elevation coordinate system [11]. Conversely, Fig. 10(b) contains the aperture illumination function of the antenna [11] where a single faulty element can be seen in the lower right-hand side of the aperture. This element, which was covered in conducting tape, can be seen in Fig. 9. above. It is important to note that these are only preliminary test results and a detailed treatment of the test system and its accuracies is planned for a future paper.

V. SUMMARY AND CONCLUSIONS

This paper has described the ongoing implementation of a new, sophisticated, very flexible, antenna measurement facility that is predicated on the use of dual 6-axis industrial robots. As has been highlighted, the rapid development and implementation of this new test system has been greatly aided by MBSE/MBD systems engineering concepts and the use of a digital twin. This has been used to drive design decisions early on during the development process and has provided a solid basis upon which high cost decisions could be made, *e.g.* as what type of absorber to use and what layout to employ. It has also enabled the evaluation of individual components within the system as well as establishing the form and magnitude of the interactions between those various subsystems. Furthermore, it has been used to provide an indication of overall system performance.

The models that have been developed have been employed to perform sensitivity analysis that would otherwise have been too costly or time prohibitive to perform experimentally, and have been used to establish system performance and perform feasibility studies for new and complex scan geometries far before the time when actual hardware would have become available. However, perhaps one of the most important attributes has been the ability to develop and validate new data post processing methodologies without the need for time consuming and expensive data collection. This has been especially crucial in the successful development of the new extrapolation gain measurement and post-processing capability that would otherwise have been far more difficult, time consuming, and expensive to complete.

ACKNOWLEDGMENT

The authors would like to thank Zhong Chen of ETS Lindgren for his help and assistance during the preparation of this paper, and for providing some of the simulations that have supported and advanced this paper and project.

REFERENCES

[1] J.A. Estefan, “Survey of model-based systems engineering (MBSE) methodologies.”, Incose MBSE Focus Group 25 (2007): 8.

[2] M. Grieves, “Digital Twin: Manufacturing Excellence through Virtual Factory Replication”, 2015.

[3] D. Novotny, et al, “Performance evaluation of a robotically controlled millimeter-wave near-field pattern range at the NIST”, 2013 7th European Conference on Antennas and Propagation

[4] J. Guerrieri, et al, “Configurable Robotic Millimeter-Wave Antenna Facility”, 2015 9th European Conference on Antennas and Propagation

[5] J Guerrieri, et al, “Validation of Robotics for Antenna Measurements”, 2017 11th European Conference on Antennas and Propagation

[6] D. R. Novotny, J. A. Gordon, M. S. Allman, “The Multi-Robot Large Antenna Positioning System for Over- The-Air Testing at the National Institute of Standards and Technology”, Proceedings of the AMTA Symposium.

[7] A. Repjar, A. Newell, and D. Tamura, “Extrapolation Range Measurements for Determining Antenna Gain and Polarization”, NIST (NBS) Technical note 1311, August 1987.

[8] A. Newell, R. Baird and P. Wacker, "Accurate measurement of antenna gain and polarization at reduced distances by an extrapolation technique," in *IEEE Transactions on Antennas and Propagation*, vol. 21, no. 4, pp. 418-431, July 1973.

[9] D. Gentle, “The removal of the effects of multiple reflections in antenna extrapolation data by digital filtering”, NPL Report DES 139, ISSN 0143-7305 , April, 1995.

[10] D. G. Gentle, P. R. Miller, “Antenna Calibrations at NPL”, Proc. AMTA 99 October, 1999.

[11] S.F. Gregson, J. McCormick, C.G. Parini, “Principles of Planar Near-Field Antenna Measurements”, IET press 2007.